Journal of Fluorescence, Vol. 13, No. 1, January 2003 (© 2003)

Effects of Metallic Silver Particles on Resonance Energy Transfer Between Fluorophores Bound to DNA

Joseph R. Lakowicz,[1,3] Józef Kuśba,[2] Yibing Shen,[1] Joanna Malicka,[1] Sabato D'Auria,[1] Zygmunt Gryczynski,[1] and Ignacy Gryczynski[1]

Received May 13, 2002; revised June 21, 2002; accepted June 27, 2002

We examined the effects of metallic silver island films on resonance energy transfer (RET) between a donor and acceptor bound to double helical DNA. The donor was 4′,6-diamidino-2-phenylindole (DAPI) and the acceptor was propidium iodide (PI). Proximity of the labeled DNA to the silver particles resulted in a dramatic increase in RET as seen from the emission spectra and the donor decay times. Proximity to silver particles results in an increase of the Förster distance from 35 Å to an apparent value of 166 Å. These results suggest a new type of DNA hybridization assays based on RET over distances much longer than the free-space Forster distance.

KEY WORDS: Radiative decay engineering; fluorescence resonance energy transfer; silver nanoparticles; labeled DNA.

INTRODUCTION

Fluorescence resonance energy transfer (RET)[4] is widely used in studies of biological macromolecules, medical research, and clinical testing. The use of RET in studies of biological structures has been reviewed [1–4]. RET is used to study protein folding and assembly [5–6]. RET is also frequently used to study membranes [7,8] and carbohydrates [9,10]. In addition to these structural applications, RET is now widely used to study a wide range of macromolecule associated reactions, including DNA hybridization [11,12], DNA folding [13–16], protein clustering in membranes [17], calcium indicators [18], proximity imaging on cells [19], and immunoassays [20,21]. In all cases the usefulness of RET is determined by the magnitude of the Förster distance (R_0). For the most favorable case of high spectral overlap and high donor (D) quantum yield, the maximum value of R_0 is near 55 Å for organic fluorophores and up to 90 Å for lanthanide donors [22–24]. Because of the upper limit on R_0 it is difficult to use RET in sandwich immunoassays when the Ds and acceptors (As) may be more than 100 Å apart. Also, for RET between Ds and As in DNA must be spaced more closely than ~30 base pairs.

We now describe a new approach to increasing the distance for RET. It is known that metallic surfaces and subwavelength size metallic particles can alter the spectral properties of fluorophores [25–27]. More specifically, fluorophores close to metallic particles have been predicted to display increased rates of radiative decay [28–31] and increased rates of resonance energy transfer [32,33]. In the case of RET the rate of energy transfer has been predicted to increase by 100-fold at distances up to 700 Å, or 10-fold larger than the Förster distances

[1] University of Maryland Baltimore, Center for Fluorescence Spectroscopy, Department of Biochemistry and Molecular Biology, 725 W. Lombard St., Baltimore, Maryland 21201.
[2] Technical University of Gdańsk, Faculty of Applied Physics and Mathematics, ul. Narutowicza 11/12, 80-952 Gdańsk, Poland.
[3] To whom correspondence should be addressed. E-mail: lakowicz@cfs.umbi.umd.edu

[4] ABBREVIATIONS: A, acceptor; D, donor; DAPI, 4′,6-diamidino-2-phenylindole; PI, propidium iodide; RET, resonance energy transfer.

1053-0509/03/0100–0069/0

in bulk solution. The expected effects of metallic surfaces on fluorescence have recently been reviewed [34] and some of these effects experimentally confirmed [35]. In the present report we examine the effects of silver island films on RET between Ds and As bound to double helical DNA.

MATERIALS AND METHODS

Calf thymus DNA was obtained from Sigma and dissolved in 50 mM Tris buffer, pH 7, to a concentration of 2 mM in base pairs using 13,300 M^{-1} cm^{-1} per base pair. DAPI and propidium iodide (PI) were obtained from Molecular Probes. Both probes bind noncovalently to DNA. PI is an intercalator and DAPI binds to the minor groove. For the energy transfer measurements the DAPI and PI concentrations were 1.5×10^{-5} M and 0.35×10^{-4} to 2.62×10^{-4} M, respectively. The DAPI concentration results in 133 base pairs per DAPI molecule. For time-resolved measurements the PI concentration was 1.5×10^{-4} M, or 13 base pairs per PI molecule.

Procedure for Making Silver Nanoparticle Films

Silver islands were formed on quartz microscope slides [36]. The use of quartz provided UV transmission and less autofluorescence than glass. The quartz slides were soaked in a 10:1 (v/v) mixture of H_2SO_4 (95–98%) and H_2O_2 (30%) overnight before the deposition. The slides were washed with distilled water and air-dried before use. Silver deposition was carried out in a clean 30-ml beaker with a Teflon-coated stir bar. To a fast stirring silver nitrate solution (0.22 g in 26 ml of Millipore water), eight drops of fresh 5% NaOH solution were added. Dark-brownish precipitates formed immediately. Less than 1 ml of ammonium hydroxide was then added drop by drop to redissolve the precipitates. The clear solution was cooled to 5°C on an ice bath, followed by soaking the cleaned and dried quartz slides in this solution. At 5°C, a fresh solution of D-glucose (0.35 g in 4 ml of water) was added. The mixture was stirred for 2 min. Subsequently, the beaker was removed from the ice bath and allowed to warm up to 30°C. The color of the mixture turned from yellow-greenish to yellow-brown. The color of the slides became greenish. The slides were removed and washed with water and bath sonicated for 1 min at room temperature. After rinsing with water the slides were stored in water for several hours before the experiments.

Emission spectra were obtained using a SLM 8000 spectrofluorometer using 360 nm excitation. Intensity decays were measured in the frequency-domain using instrumentation described previously [37,38]. The excitation wavelength of 360 nm was obtained from the frequency-doubled output of a 3.80-MHz cavity dumped Pyridine 2 dye laser with a 10 ps or less pulse width.

For the frequency-domain measurements the emission was observed through a 460 nm interference filter. For all steady state and frequency-domain (FD) measurements the excitation was vertically polarized and the emission was observed through a horizontally oriented polarizer to minimize scattered light. The FD intensity decay were analyzed in terms of the multiexponential model

$$I(t) = \sum_i \alpha_i \exp(-t/\tau_i) \tag{1}$$

where τ_i are the lifetimes with amplitudes α_i and $\Sigma\ \alpha_i = 1.0$. Fitting to the multiexponential model was performed as described previously [39]. The contribution of each component to the steady state intensity is given by

$$f_i = \frac{\alpha_i \tau_i}{\sum_j \alpha_j \tau_j} \tag{2}$$

The mean decay time is given by

$$\bar{\tau} = \sum_i f_i \tau_i \tag{3}$$

The amplitude-weighted lifetime is given by

$$\langle \tau \rangle = \sum_i \alpha_i \tau_i \tag{4}$$

There is frequently confusion about the use of lifetimes to determine the transfer efficiency. Let $I_D(t)$ and $I_{DA}(t)$ represent the intensity decay of the D in the absence and presence of the A, respectively. The transfer efficiency (E) can be calculated from the integrated area under the intensity decays

$$E = 1 - \frac{\int I_{DA}(t)dt}{\int I_D(t)\,dt} \tag{5}$$

After analysis in terms of the multiexponential model (Eq. 1), these areas are proportional to the amplitude-weighted lifetimes calculated using Equation 4. Hence, the transfer efficiency is given by

$$E = 1 - \frac{\langle \tau_{DA} \rangle}{\langle \tau_D \rangle} \tag{6}$$

where $\langle \tau_{DA} \rangle$ and $\langle \tau_D \rangle$ are calculated from the multiexponential analysis of the D decays in the absence and presence of A, respectively.

THEORY

Single Forster Distance

The rate of RET between a D and an A is given by

$$k(r) = \frac{1}{\tau_0}\left(\frac{R_0}{r}\right)^6 \tag{7}$$

where τ_0 is the donor decay time in the absence of A, r is the D-to-A distance, and R_0 is the Forster distance at which the rate of energy transfer is equal to the inverse decay rate ($1/\tau_0$) or equivalently the distance at which RET is 50% efficient. One can assume that in the case of Ds and As randomly bound to DNA, the D intensity decay is given by [40–42]

$$I_D(t) = \sum_i \alpha_i \varphi_i(t) \tag{8}$$

where

$$\ln\varphi_i(t) = -\frac{t}{\tau_i} + \frac{\rho}{C_0}\left(\frac{t}{\tau_i}\right)^{1/6} \sum_{k=1}^{\infty} \frac{1}{k}\left(\frac{C_A}{\rho}\right)^k \left[\lambda_i^{-1/6}(1 - e^{-\lambda_i})^k + \sum_{L=1}^{k} (-1)^L \binom{k}{L} L^{1/6}\gamma\left(\frac{5}{6}, L\lambda_i\right)\right] \tag{9}$$

Equation 9, where τ_i are the decay times associated with each component in the D decay (Eq. 1), assumes the Ds and As are distributed on a one-dimensional lattice, where $C_0 = (2R_0)^{-1}$ and C_A is the A concentration, ρ is the density of lattice points, $\lambda_i = (t/\tau_i)(R_0/r_{min})^6$ with r_{min} denoting the minimum D-A distance, and $\gamma(a,x)$ is the incomplete gamma function. In this analysis we use the intensity decay of the D in the absence of A (α_i and τ_i values) are fixed parameters.

For the initial analysis we used Eq. 6 to calculate the single apparent value of R_0 using the known A density as a constant. If the A concentration is known, the D decay can be used to determine the Forster distance R_0. The fixed parameters were the base pair length 3.4 Å and r_{min} = 12 Å. Additional details are available [41,42].

Two Forster Distances

We analyzed the data in terms of two Forster distances, one assigned to the bulk solution (R_{01}) and the second due to Ds and As in close proximity to the silver particles (R_{02}). In this case the intensity decay was given by

$$I_D(t) = g_1 \sum_i \alpha_i \varphi_{i1}(t) + g_2 \sum_i \alpha_i \varphi_{i2}(t) \tag{10}$$

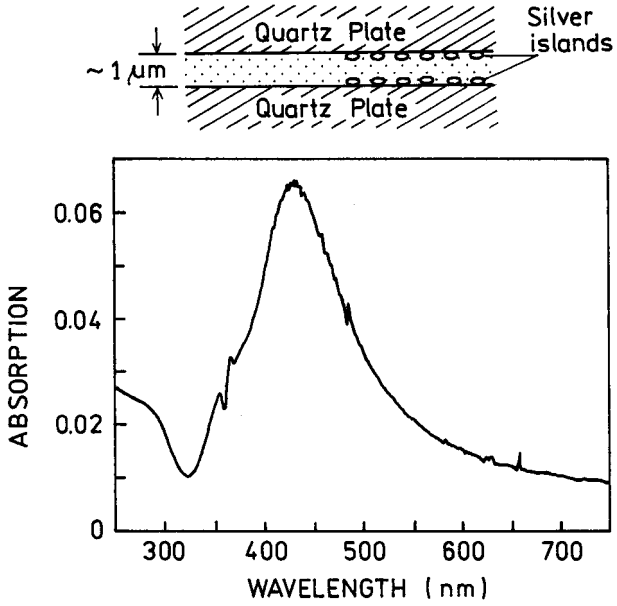

Fig. 1. Absorption spectra of the silver island films on a quartz slide. The top figure shows the experimental geometry.

where $\varphi_{i1}(t)$ and $\varphi_{i2}(t)$ refer to the populations with R_{01} and R_{02}, respectively. The decay functions $\varphi_{i1}(t)$ and $\varphi_{i2}(t)$ were calculated using the expression

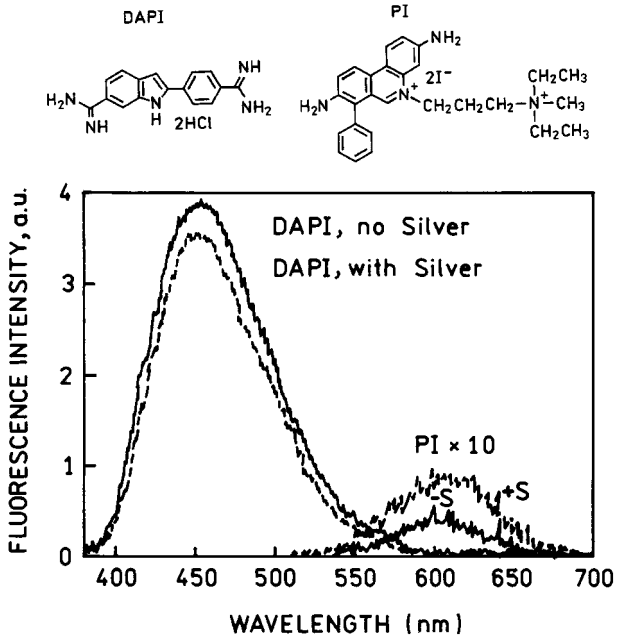

Fig. 2. Emission spectra of DAPI-labeled DNA and PI-labeled DNA between two silver island films. The DNA concentration was 2 mM/bp. The concentrations of DAPI and PI were 1.5×10^{-5} M (0.0075/bp) and 1.5×10^{-4} (0.075/bp), respectively.

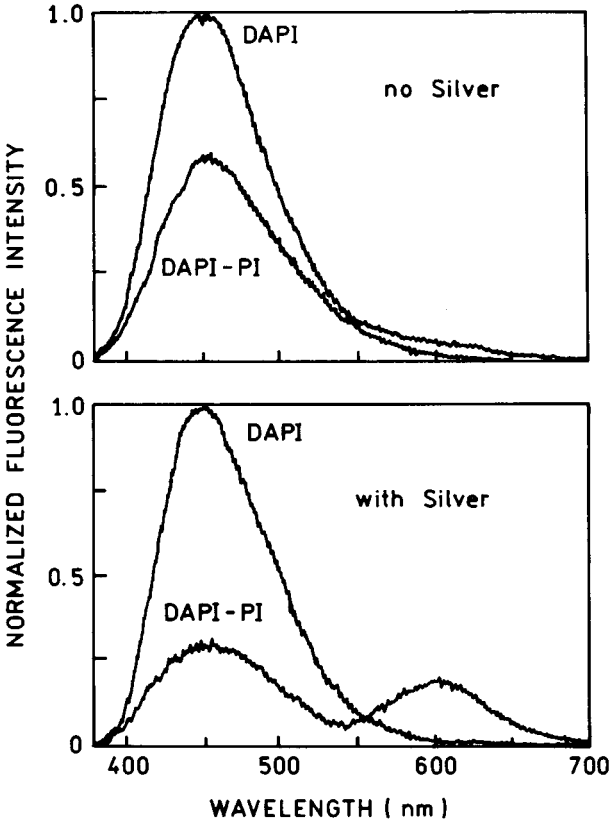

Fig. 3. Emission spectra of DAPI-labeled DNA (donor) and DAPI-PI labeled DNA donor-acceptor on quartz (top) and silver island film (bottom). The concentration of PI was 150 μm.

$$\log \varphi_{ij}(t) = -\frac{t}{\tau_i} + \frac{\rho}{C_{0j}}\left(\frac{t}{\tau_i}\right)^{1/6} \sum_{k=1}^{\infty} \frac{1}{k}\left(\frac{C_A}{\rho}\right)^k \left[\lambda_{ij}^{-1/6}(1 - e^{-\lambda_{ij}})^k + \sum_{L=1}^{k} (-1)^L \binom{k}{L} L^{1/6} \gamma\left(\frac{5}{6}, L\lambda_{ij}\right)\right] \quad (11)$$

with $C_{0j} = (2R_{0j})^{-1}$ $\lambda_{ij} = (t/\tau_i)(R_{0j}/r_{min})^6$. We assumed that the D decay times τ_i were the same for both populations. The quantities g_1 and g_2 represent the time zero amplitudes of the intensity decays of the respective populations and were normalized so that $g_1 + g_2 = 1$. The relative contributions of the time-integrated intensity decays were calculated as

$$F_j = \frac{g_j \sum_i \alpha_i \int_0^\infty \varphi_{ij}(t)\, dt}{\int_0^\infty I_D(t)\, dt} \quad (12)$$

where $I_D(t)$ is given by Eq. (10) (It is easy to see that $F_1 + F_2 = 1$.)

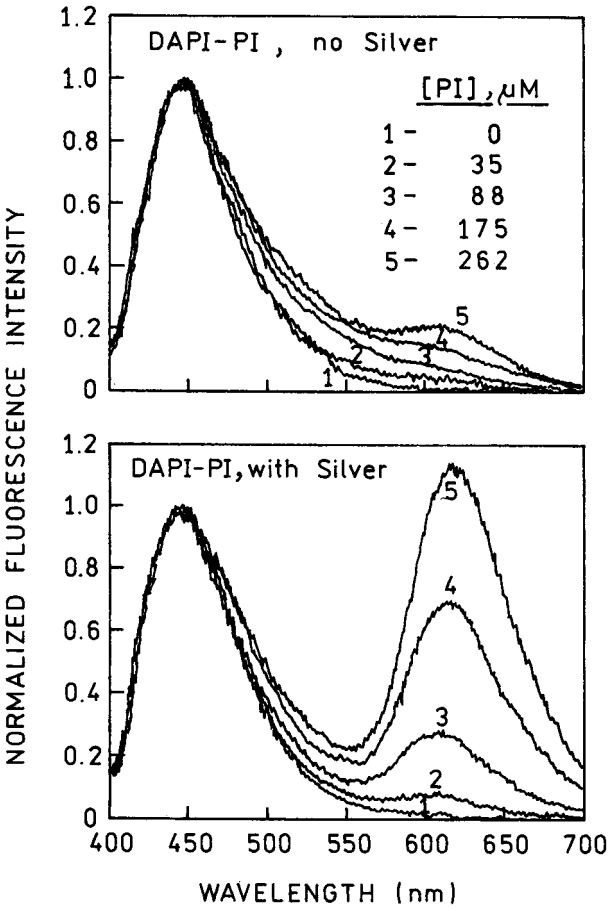

Fig. 4. Donor-normalized emission spectra of DAPI-PI labeled DNA for various PI acceptor concentrations.

RESULTS

Silver particles were obtained by chemical reduction of silver onto quartz slides [36]. If the mass thickness of the deposited silver is kept near 40 Å the silver particles have subwavelength dimensions and display a characteristic surface plasmon absorption (Fig. 1). From studies of the absorption spectra of dyes between two such silver island films we found the sample thickness to be near 1 to 1.5 μm [35].

To study the effect of silver islands on resonance energy transfer we used double helical calf thymus DNA that was labeled with Ds and As. All labeled DNA were in the double helical form. The Ds-alone DNA is DAPI-DNA, the A-alone DNA is PI-DNA, and the DNA labeled with both D and A is referred to as DAPI-PI-DNA.

The effects of the silver island films on DNA labeled with only the DAPI D or only the PI A are shown in Figure 2. In the case of DAPI-DNA the intensity is only slightly changed when placed between quartz plates or

between silver island films. An unchanged intensity is expected for high quantum yield fluorophores [35]. In the case of PI-DNA there is a ~2-fold increase in the PI intensity. With the 360 nm excitation wavelength for the D, the A absorbs weakly and the directly excited A emission is negligible. The larger effect of the silver island film on PI-DNA is consistent with its lower quantum yield near 0.15 compared with 0.53 for DAPI-DNA [42]. It is known that metallic surfaces can increase the intensity of low quantum yield fluorophores and that the maxi-

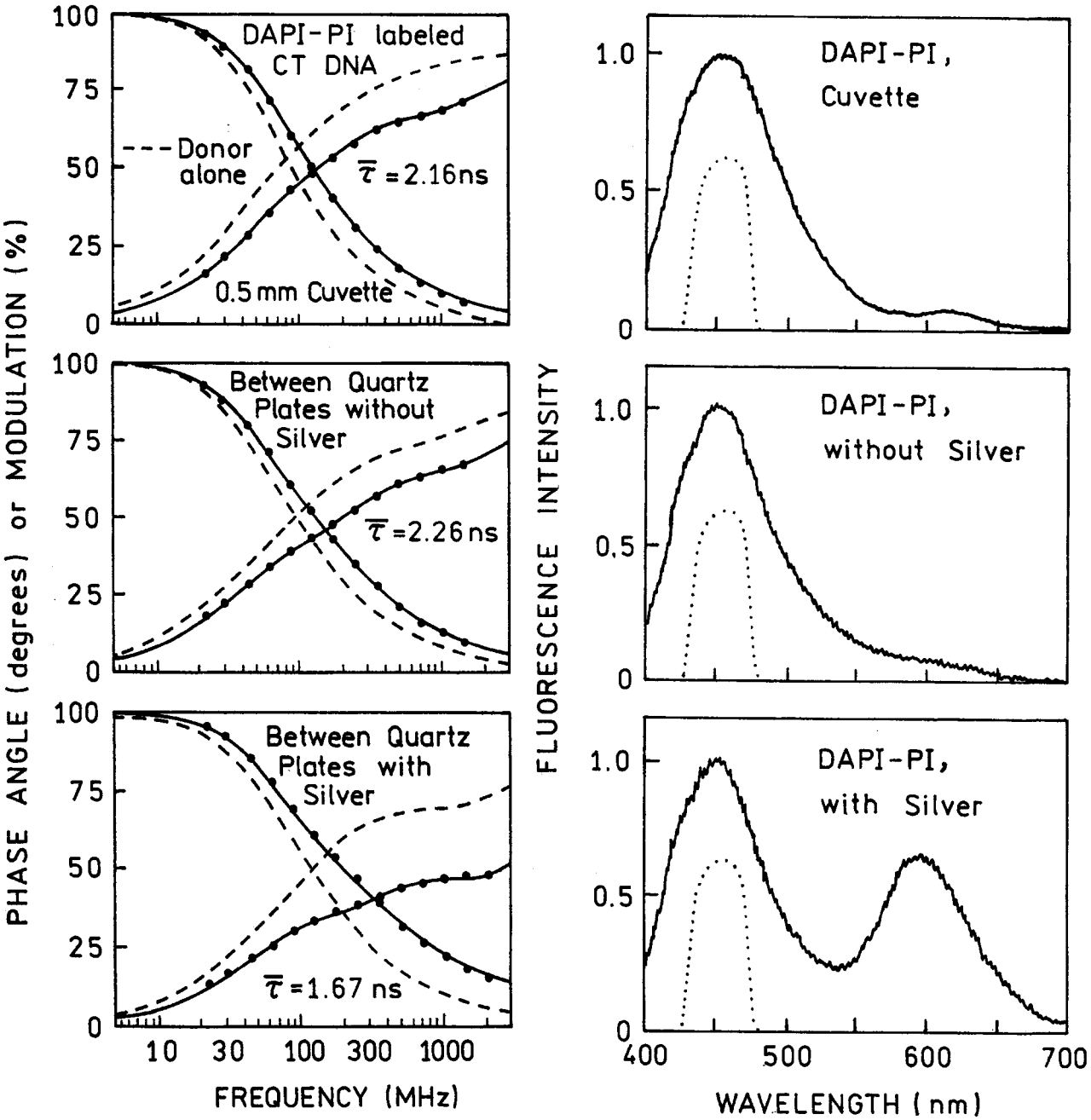

Fig. 5. Left: Frequency-domain intensity decays of the DAPI donor decay for DNA labeled with both DAPI and PI. Each panel shows the decay of the DAPI-labeled DNA (no PI) as dashed lines. The concentration of PI was 150 μM (0.075 per base pair). Right: Normalize emission spectra of DAPI-PI labeled DNA. The dotted line is the transmission of observation filter.

mum enhancement is 1/Q, where Q is the quantum yield in the absence of metal [29]. The extent of energy transfer is consistent with the R_0 value of ~35 Å for this D-A pair [42]. Based on the extent of A labeling of 1 per 13 base pairs, and 3.4 Å per base pair in the DNA helix, the A molecules are on average 45 Å apart.

Next, we examined DAPI-DNA donor and DAPI-PI-DNA D-A system between quartz plates without and with silver island films. The spectra in Figure 3 clearly shows a larger decrease of the D emission in presence of silver islands. Consequently, the PI A displays stronger sensitized emission on silver islands than on quartz only (Fig. 3). However, it is difficult to calculate the energy transfer efficiency from these spectral data. In our front-face geometry used for measurements, even small displacements may cause additional errors in the intensity reading. In contrast the lifetime measurements are practically independent on experimental geometry. We also present energy transfer effects in ratiometric form, where the spectra are normalized to the D emission (Fig. 4). Calculation of energy transfer will be done directly from lifetime measurements.

The emission spectra of D-A-labeled DNA are shown in Figure 4 for various PI concentrations. As the PI concentration increased, its emission become stronger for both without and with silver samples. However, the emission from PI in the presence of the silver island films is ~5-fold more intense. The silver island film had a smaller 2-fold effect on A-only DNA (PI-DNA). These results suggest an increase in the efficiency of RET from DAPI to PI due to proximity to the silver islands.

An increase in energy transfer from DAPI to PI is expected to result in a decrease in the DAPI decay time. Frequency-domain intensity decays of the DAPI donor are shown in Figure 5. The dashed lines in each panel show the DAPI decays in the absence of the PI A. In the absence of silver islands the D-alone amplitude-weighted decay time $\langle\tau_D\rangle = 1.58$ ns was reduced to $\langle\tau_{DA}\rangle = 0.80$ ns in the presence of PI, suggesting a transfer efficiency of 49% (Table I). In the presence of silver islands the amplitude-weighted decay time is reduced from $\langle\tau_D\rangle = 1.10$ ns to $\langle\tau_{DA}\rangle = 0.24$ ns, which corresponds to a transfer efficiency of 78%. Control measurements showed the absence of scattered light in all these measurements. The increase in energy transfer also suggests the DNA remains in the double helical form in the presence of silver islands. If the double helix were disrupted, the probes would no longer bind to DNA and the extent of energy transfer would decrease.

We analyzed the frequency-domain D decays in terms of the apparent Forster distance. This was accomplished by analyzing the D decay using Eq. 8. The A concentration was held constant at 0.075 A per base pair and the values of R_0 were allowed to vary to obtain the best fit to the data (Fig. 6). The value of $R_0 = 32.5$ Å obtained for quartz plates without silver is close to that calculated for this D-A pair, $R_0 = 35.7$ Å. Importantly, the apparent value of R_0 increased more than 2-fold to 73.6 Å for the sample between the silver island films. We note that this is an apparent R_0 value. Examination of this fit (Fig. 6, lower panel) reveals that the frequency-domain intensity decay could not be fit to a single R_0 value. This suggests the presence of at least two populations of D-A pairs, with the pairs at optimum distance to the silver islands displaying a larger R_0 value. It is important to recognize that the 2-fold increase in the apparent value of R_0 represents a minimum estimate of the effect of the silver islands on RET. We expect the active space near the silver islands extend ~200 Å into the solution. Assuming a sample thickness of 1 μm, only ~4% of the sample is within the active value. We believe the fraction of the total emission from the D-A pairs close to the silver islands is greater than 4% due to selective excitation near the particles due to the concentrated exci-

Table I. Multiexponential Analysis of DAPI Donor Intensity Decay in the Presence and Absence of Acceptor and Silver Islands

Sample[a]	$\bar{\tau}$ (ns)	$\langle\tau\rangle$ (ns)	E	α_1	τ_1 (ns)	α_2	τ_2 (ns)	α_3	τ_3 (ns)	χ^2_R
DAPI-DNA, Q	2.80[b]	1.58[c]		0.311	0.16	0.391	1.15	0.298	3.62	1.2[d]
DAPI-DNA, S	2.39	1.10		0.447	0.09	0.414	1.29	0.139	3.70	1.1
DAPI-PI-DNA, Q	2.26	0.80	0.49[e]	0.467	0.08	0.367	0.66	0.166	3.15	1.0
DAPI-PI-DNA, S	1.67	0.24	0.78	0.769	0.04	0.172	0.40	0.059	2.44	1.7

[a] Q̂, Between quartz plates without silver; S, between quartz plates with silver.
[b] $\bar{\tau} = \Sigma\, f_i\, \tau_i$.
[c] $\langle\tau\rangle = \Sigma\, \alpha_i\, \tau_i$.
[d] The uncertainties in the phase angles and modulations, for the least squares analysis, were taken as ${}_4\sigma_p = 0.4°$, $\sigma_m = 0.01$, respectively.
[e] $E = 1 - \dfrac{\langle\tau_{DA}\rangle}{\tau_D}$.

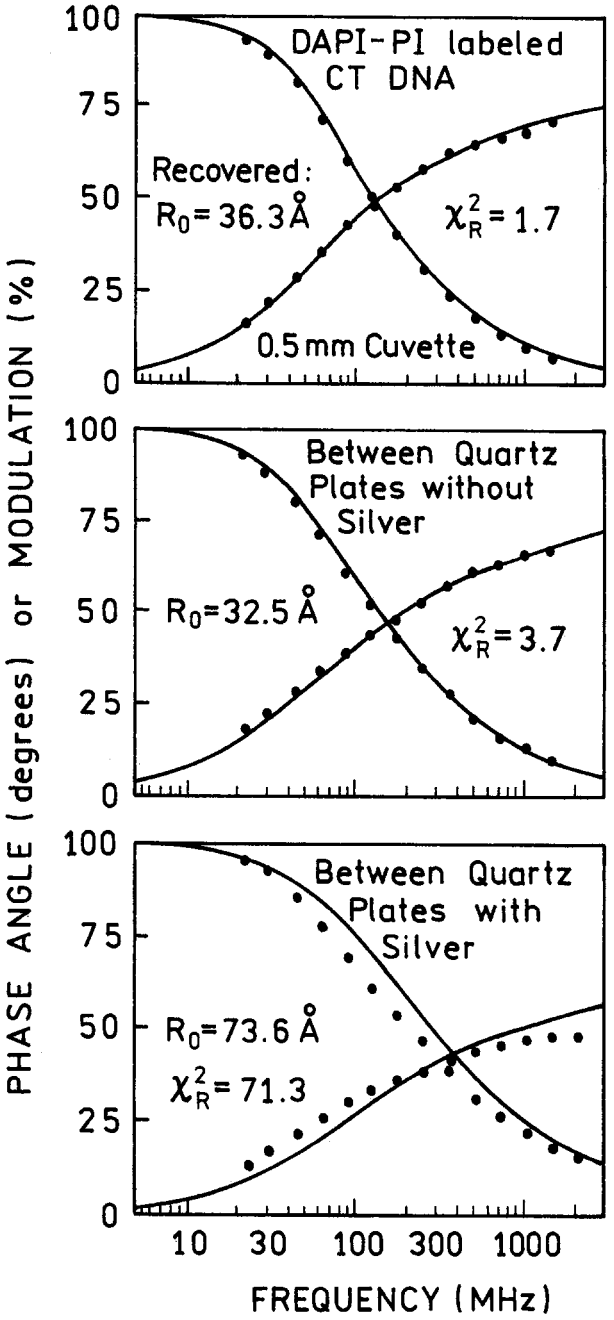

Fig. 6. Frequency-domain intensity decays of DAPI in DNA labeled with both DAPI and PI. The FD data were analyzed to obtain the best fit to a single R_0 value.

tation field and due to an increased quantum yields of DAPI near the silver islands. Because a minor fraction of the DAPI emission is from the molecules close to silver, these results suggest that the actual effect on RET is greater than a 2-fold increase in R_0 for those molecules adjacent to the silver particles.

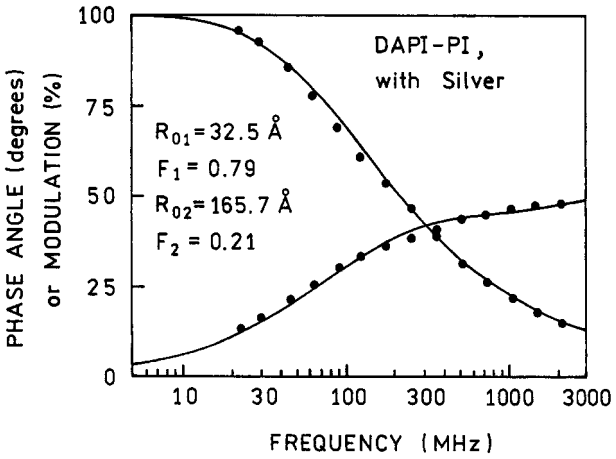

Fig. 7. Energy transfer analysis of the frequency-domain data in terms of two populations of DAPI-PI labeled DNA with different R_0 values.

We analyzed the frequency-domain D decay for the sample between silver island films in terms of two Forster distances (Fig. 7). The value of R_{01} was held constant at the values found for the sample between the quartz plates without silver island films. The use of a second Forster distance, R_{02}, resulted in a greatly improved fit with the value of χ^2_R decreasing more than 10-fold from 71.3 to 6.4 (Table II). The second R_0 value was found to be remarkably large, 165.7 Å. Examination of the χ^2_R surface (Fig. 8) showed that this value was determined with good certainty from the data and is most likely to be within the range from 158 to 176 Å. This range of values was calculated for one standard deviation ($P = 0.32$) with two variable parameters and 25 degrees of freedom [43]. We note that the sample is characterized by a range of distances of the DNA from the metal particles, so that this second larger R_0 value represents a weighted average of the R_0 values for our experimental configurations.

The recovered fraction of molecules with a larger R_0 value (21%) is larger than the estimated active volume near the silver island film (4%). Possibly, other effects such as microcavities created by two silvered slides play an additional role.

Table II. Energy Transfer Analysis of DAPI-PI Labeled DNA

	One R_0 Model		Two R_0 Model			
Condition	R_0 (Å)	χ^2_R	R_{01} (Å)	R_{02} (Å)	F_1[a]	χ^2_R
Quartz	32.5	3.7	—	—	—	—
Silver	73.6	71.3	⟨32.5⟩[b]	165.7	0.79	6.4

[a] Fractional intensity, $F_2 = 1 - F_1$.
[b] Angular brackets indicate a fixed parameter value.

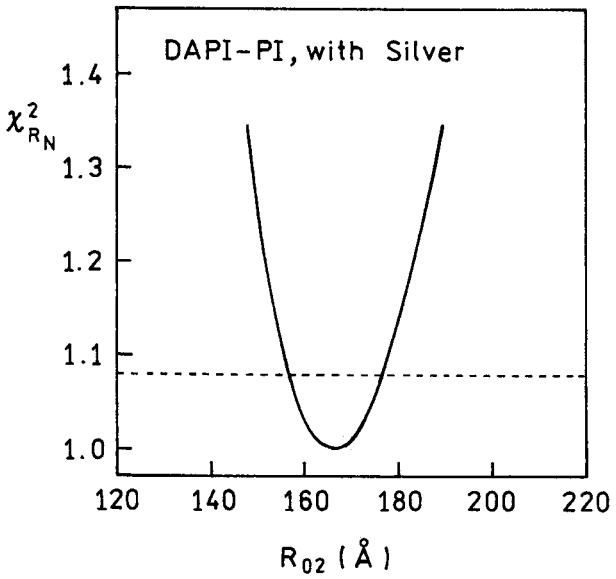

Fig. 8. The resolution of recovered enhanced Forster distance R_{02} as seen by the χ^2_R surfaces. The value of R_{01} was kept constant at the value recovered in absence of silver (see Table II) while fractional intensity g_2 was floating.

DISCUSSION

Increases in energy transfer near metallic particles can have many applications in the biomedical uses of fluorescence. For instance, immunoassays are infrequently performed using RET because the large size of immunoglobulin, relative to the R_0 values, results in minimal energy transfer. At present, the commercial uses of RET in biochemical assays are limited to the use of lanthanide Ds and gated detection of As to isolate the small signals from RET-excited acceptors [44,45]. The use of assay chambers coated with or containing metallic particles could result in efficient RET even between D and As over 100 Å apart. Another possibility is the use of metal enhanced energy transfer with DNA arrays or gene chips. At present the arrays are read by measuring the amount of two fluorophores hybridized to the target DNA [46–48]. Even though the two dyes are often a good D-A pair, energy transfer does not normally occur. The use of DNA arrays on metallic surfaces could provide a new type of DNA array analysis based on RET between Ds and As positioned at long distances. However, without precise control of the particle dimensions and location of the fluorophores, the RET data will not yield values for the D-A distance.

Many additional applications of metal-enhanced RET can be imagined. For instance, this effect could be used increasing the efficiency of light harvesting assemblies based on RET [49,50] or to increase the extent of RET between Ds and As within cells [51,52] but close to metallic particles. The phenomenon of metal-enhanced RET provides a unique opportunity of using the proximity of D-A pairs to metallic particles to modify the rates of transfer. Such effects are unique because the metal particles or surfaces, rather than the solution composition, can be used to modify the extent of energy transfer.

REFERENCES

1. L. Stryer (1978) Fluorescence energy transfer as a spectroscopic ruler. *Annu. Rev. Biochem.* **47**, 819–846.
2. D. M. J. Lilley and T. J. Wilson (2000) Fluorescence resonance energy transfer as a structural tool for nucleic acids. *Curr. Opin. Chem. Biol.* **4**, 507–517.
3. C. G. Dos Remedios and P. D. J. Moens (1995) Fluorescence resonance energy transfer spectroscopy is a reliable "ruler" for measuring structural changes in proteins. *J. Struct. Biol.* **115**, 175–185.
4. P. Wu and L. Brand (1994) Review-resonance energy transfer. Methods and applications. *Anal Biochem.* **218**, 1–13.
5. D. S. Talaga, W. L. Lau, H. Roder, J. Tang, Y. Jia, W. F. DeGrado, and R. M. Hochstrasser (2000) Dynamics and folding of single two-stranded coiled-coil peptides studied by fluorescent energy transfer confocal microscopy. *PNAS* **97**, 13021–13026.
6. E. B. Getz, R. Cooke, and P. R. Selvin (1998) Luminescence resonance energy transfer measurements in myosin. *Biophys. J.* **74**, 2451–2458.
7. J. Matko and M. Edidin (1997) Energy transfer methods for detecting molecular clusters on cell surfaces. *Methods in Enzymol.* **278**, 444–462.
8. H. Laguitton-Pasquier, M. Van der Auweraer, and F. C. De Schryver (1998) Bidimensional distribution of a cyanide dye in Langmuir-Blodgett (LB) monolayers studied by time-resolved and spatially resolved fluorescence. *Langmuir* **14**, 5172–5183.
9. Y. C. Lee (1997) Fluorescence spectrometry in studies of carbohydrate-protein interactions. *J. Biochem.* **121**, 818–825.
10. M. P. Brown, D. Toptygin, K. B. Lee, T. Animashaun, R. C. Hughes, Y. C. Lee, and L. Brand (1998) The tryptophan fluorescence of *Tetracarbidium conophorum* agglutinin II and a solution-based assay for the binding of a biantennary glycopeptide. *J. Protein Chem.* **17**, 149–159.
11. M. Masuko, S. Ohuchi, K. Sode, H. Ohtani, and A. Shimadzu (2000) Fluorescence resonance energy transfer from pyrene to perylene labels for nucleic acid hybridization assays under homogenous solution conditions. *Nucleic Acids Res.* **28**, e34.
12. S. Sueda, J. Yuan, and K. Matsumoto (2000) Homogenous DNA hybridization assay by using europium luminescence energy transfer. *Bioconjugate Chem.* **11**, 827–831.
13. T. Mitsui, H. Nakano, and K. Yamana (2000) Coumarin-fluorescein pair as a new donor-acceptor set for fluorescence energy transfer study of DNA. *Tetrahedron Letts.* **41**, 2605–2608.
14. D. G. Norman, R. J. Grainger, D. Uhrin, and D. M. J. Lilley (2000) Location of cyanine-3 on double-stranded DNA: Importance for fluorescence resonance energy transfer studies. *Biochem.* **39**, 6317–6324.
15. F. Walter, A. I. H. Murchie, D. Duckett, and D. M. J. Lilley (1998) Global structure of four-way RNA junctions studied using fluorescence resonance energy transfer. *RNA* **4**, 719–728.
16. M. Yang, L.-Q. Ren, M. Huang, R. Y. C. Kong, and W. F. Fong (1998) A DNA assay based on fluorescence resonance energy transfer and DNA triplex formation. *Anal. Biochem.* **259**, 272–274.
17. U. Kubitscheck, M. Kircheis, R. Schweitzer-Stenner, W. Dreybrodt, T. M. Jovin, and I. Pecht (1991) Fluorescence resonance energy

transfer on single living cells. Application to binding of monovalent haptens to cell-bound immunoglobulin E. *Biophys. J.* **60**, 307–318.
18. A. Miyawaki, J. Llopis, R. Helm, J. M. McCaffrey, J. A. Adams, M. Ikura, and R. Y. Tsien (1997) Fluorescent indicators for Ca^{2+} based on green fluorescent proteins and calmodulin. *Nature* **388**(28), 882–887.
19. D. A. De Angelis, G. Miesenböck, B. V. Zemelman, and J. E. Rothman (1998) PRIM: Proximity imaging of green fluorescent protein-tagged polypeptides. *Proc. Natl. Acad. Sci. USA* **95**, 12312–12316.
20. E. F. Ullman, M. Schwarzberg, and K. E. Rubenstein (1976) Fluorescent excitation transfer immunoassay: A general method for determination of antigens. *J. Biol. Chem.* **251**, 264–270.
21. U. Schobel, H.-J. Egelhaaf, A. Brecht, D. Oelkrug, and G. Gauglitz (1999) New donor-acceptor pair for fluorescent immunoassays by energy transfer. *Bioconj. Chem.* **10**, 1107–1114.
22. P. R. Selvin, T. M. Rana, and J. E. Hearst (1994) Luminescence resonance energy transfer. *J. Am. Chem. Soc.* **116**, 6029–6030.
23. P. R. Selvin (1996) Lanthanide-based resonance energy transfer. *IEEE J. Selected Topics in Quantum Electron.* **2**, 1077–1087.
24. G. Mathis (1993) Rare earth cryptates and homogenous fluoroimmunoassays with human sera. *Clin. Chem.* **39**, 1953–1959.
25. K. H. Drexhage (1974) Interaction of light with monomolecular dye lasers, Chapter IV in E. Wolf (Ed.). *Progress in Optics XII*, North-Holland, Amsterdam-London 1974, pp. 161–232.
26. E. A. Hinds (1991) Cavity quantum electrodynamics. *Advances in Atom. Molec. and Opt. Phys.* **28**, 237–289.
27. R. R. Chance, A. Prock, and R. Silbey (1978) Molecular fluorescence and energy transfer near interfaces. *Adv. Chem. Phys.* **37**, 1–65.
28. D. A. Weitz and S. Garoff (1983) The enhancement of Raman scattering, resonance Raman scattering, and fluorescence from molecules adsorbed on a rough silver surface. *J. Chem. Phys.* **78**, 5324–5338.
29. J. Kümmerlen, A. Leitner, H. Brunner, F. R. Aussenegg, and A. Wokaun (1993) Enhanced dye fluorescence over silver island films: analysis of the distance dependence. *Molec. Phys.* **80**, 1031–1046.
30. H. Chew (1987) Transition rates of atoms near spherical surfaces. *J. Chem. Phys.* **87**, 1355–1360.
31. J. Gersten and A. Nitzan (1981) Spectroscopic properties of molecules interacting with small dielectric particles. *J. Chem. Phys.* **75**, 1139–1152.
32. X. M. Hua, J. I. Gersten, and A. Nitzan (1985) Theory of energy transfer between molecules near solid state particles. *J. Chem. Phys.* **83**, 3650–3659.
33. J. I. Gersten and A. Nitzan (1984) Accelerated energy transfer between molecules near a solid particle. *Chem. Phys. Letts.* **104**, 31–37.
34. J. R. Lakowicz (2001) Radiative decay engineering: Biophysical and biomedical applications. *Anal. Biochem.* **298**, 1–24.
35. J. R. Lakowicz, Y. Shen, S. D'Auria, J. Malicka, Z. Gryczynski, and I. Gryczynski (2002) Radiative decay engineering 2: Effects of silver island films on fluorescence intensity, lifetimes and resonance energy transfer. *Anal. Biochem.* **301**, 267–277.
36. F. Ni and T. M. Cotton (1986) Chemical procedure for preparing surface-enhanced Raman scattering active silver films. *Anal. Chem.* **58**, 3159–3163.
37. J. R. Lakowicz and B. P. Maliwal (1985) Construction and performance of a variable-frequency phase modulation fluorometer. *Biophys. Chem.* **21**, 61–78.
38. G. Laczko, I. Gryczynski, Z. Gryczynski, W. Wiczk, H. Malak, and J. R. Lakowicz (1990) A 10-GHz frequency-domain fluorometer. *Rev. Sci. Instrum.* **61**, 2331–2337.
39. J. R. Lakowicz, G. Laczko, H. Cherek, E. Gratton, and M. Limkeman (1994) Analysis of fluorescence decay kinetics from variable-frequency phase shift and modulation data. *Biophys. J.* **46**, 463–477.
40. A. Blumen and J. Manz (1979) On the concentration and time dependence of the energy transfer to randomly distributed acceptors. *J. Chem. Phys.* **71**, 4696–4702.
41. B. P. Maliwal, J. Kusba, and J. R. Lakowicz (1995) Fluorescence energy transfer in one dimension: frequency domain fluorescence study of DNA-fluorophore complexes. *Biopolymers* **35**, 245–255.
42. S.-I. Murata, J. Kusba, G. Piszczek, I. Gryczynski, and J. R. Lakowicz (2000) Donor fluorescence decay analysis for energy transfer in double-helical DNA with various acceptor concentrations. *Biopolymers (Biospectrosc.)* **57**, 306–315.
43. J. R. Lakowicz (Ed.) (1999) *Principles of Fluorescence Spectroscopy*, Kluwer Academic/Plenum Publishers, New York, 698 pp.
44. J. T. Bookout, T. R. Joaquim, M. K. Magin, G. J. Rogan, and R. P. Lirette (2000) Development of a dual-label time-resolved fluorometric immunoassay for the simultaneous detection of two recombinant proteins in potato. *J. Agric. Food Chem.* **48**, 5868–5873.
45. M. Samiotaki, M. Kwiatkowski, N. Ylitalo, and U. Landegren (1997) Seven-color time-resolved fluorescence hybridization analysis of human papilloma virus types. *Anal. Biochem.* **253**, 156–161.
46. T. L. Ferea and P. O'Brown (1999) Observing the living genome. *Curr. Opin. Genetics and Dev.* **9**, 715–722.
47. R. J. Lipshutz, S. P. A. Fodor, T. R. Gingeras, and D. J. Lockhart (1999) High density synthetic oligonucleotide arrays. *Nature Gen. Suppl.* **1**, 20–24.
48. J. G. Hacia, L. C. Brody, and F. S. Collins (1998) Applications of DNA chips for genome analysis. *Molec. Psychiatry* **3**, 483–492.
49. A. Adronov, S. L. Gilat, J. M. J. Fréchet, K. Ohta, F. V. R. Neuwahl, and G. R. Fleming (2000) Light harvesting and energy transfer in laser-dye labeled poly(aryl ether) dendrimers. *J. Am. Chem. Soc.* **122**, 1175–1185.
50. S. F. Swallen, R. Kopelman, J. S. Moore, and C. Devadoss (1999) Dendrimer photoantenna supermolecules: energetic funnels, exciton hopping and correlated excimer formation. *J. Molec. Structure* **485–486**, 585–597.
51. J. González and R. Y. Tsien (1995) Voltage sensing by fluorescence resonance energy transfer in single cells. *Biophys. J.* **69**, 1272–1280.
52. T. Ng, A. Squire, G. Hansra, F. Bornancin, C. Prevostel, A. Hanby, W. Harris, D. Barnes, S. Schmidt, H. Mellor, P. I. H. Hastiaens, and P. J. Parker (1999) Imaging protein kinase Cα activation in cells. *Science* **283**, 2085–2089.